Numerical Modeling of Antenna Transmission for Borehole Ground-Penetrating Radar —Code Development—

Han Nuree Chang[1], Hee Joon Kim[1]

[1] Dept. Environmental Exploration Eng., Pukyong National Univ., nr8073@hotmail.com

시추공 레이다를 위한 안테나 전파의 수치 모델링 —프로그램 개발—

장한누리[1], 김희준[1]

[1] 부경대학교 환경탐사공학과

Abstract: High-frequency electromagnetic (EM) wave propagation phenomena associated with borehole ground-penetrating radar (GPR) surveys are complex. To improve the understanding of governing physical processes, we present a finite-difference time-domain solution of Maxwell's equations in cylindrical coordinates. This approach allows us to model the full EM wavefield associated with borehole GPR surveys. The algorithm can be easily implemented perfectly matched layers for absorbing boundaries, frequency-dependent media, and finite-length transmitter antenna.
Keywords: borehole, GPR, finite-difference time-domain, cylindrical coordinates

요약 : 지중 레이다 탐사에서 고주파수 전자파의 전파 현상은 복잡하다. 전자파 전파에 현상을 지배하는 물리적인 과정에 대한 이해를 향상시키기 위해서, 본 논문에서는 원통좌표계 맥스웰 방정식의 시간영역 유한차분법을 소개한다. 이 접근법은 시추공 지중 레이다탐사와 관련된 전자 파동장의 전파형을 모델화할 수 있다. 이 알고리듬은 완전정합층(PML)을 통한 흡수경계, 주파수 의존성 매질, 그리고 유한 길이 송신 안테나에서 쉽게 이행될 수 있다.
주요어 : 시추공, 지중레이다, 유한차분 시간영역, 원통좌표

1. Introduction

Over the past decade, borehole ground-penetrating radar (GPR) has gained increasing popularity as a tool for high-resolution imaging of the shallow subsurface. Applications of this technique include delineation of ore bodies (Fullagar et al., 2000); location of underground tunnels and voids (Olhoeft, 1988; Moran and Greenfield, 1993); mapping fractures in bedrock (Olsson et al., 1992; Day-Lewis et al., 2003); and estimation of subsurface lithology and hydrogeologic properties using field- or laboratory-derived petrophysical relationships (Alumbaugh and Chang, 2002; Moysey and Knight, 2004; Tronicke et al. 2004).

Crosshole GPR tomography is identical in principle to seismic tomography. A transmitter antenna, moved to numerous locations in one borehole, radiates high-frequency electromagnetic (EM) pulses that are recorded by a receiver antenna, which is moved down a second borehole. Most commonly, inversion of the resulting data is accomplished by assuming that the propagating radar energy can be

modeled by infinite-frequency rays that join the centers of the antennae. Under this assumption, first-break traveltimes and amplitudes of the data can be used to determine the distribution of subsurface EM-wave velocity and attenuation. The resulting ray-based tomographic images of the subsurface, however, are limited in resolution to approximately the width of the first Fresnel zone associated with the propagating pulse bandwidth (Williamson and Worthington, 1993). In order to improve resolution, we require modeling algorithms that account for more detailed physical aspects of the crosshole GPR experiment, such as wave propagation and antenna behavior. These algorithms can be employed in waveform-based inversion strategies that use all of the recorded data to determine subsurface properties (e.g., Pratt and Worthington, 1988; Zhou et al., 1995).

There are a number of approaches for crosshole GPR modeling. None of these, however, allow for the simulation of both antenna transmission and reception in heterogeneous media. Sato and Thierbach (1991), for example, analytically modeled a crosshole GPR experiment using an expression for the current on an insulated dipole antenna derived by King and Smith (1981). Although their approach gives much insight into the effects of antenna and system parameters on recorded GPR wavelets, it requires a homogeneous medium between the boreholes and that the antennae be in the far field of one another. In addition, the expression used for the antenna current is invalid for the case of water-filled boreholes and is thus only suitable for modeling in the vadose zone. Holliger and Bergmann (2002), on the other hand, numerically modeled crosshole GPR using a finite-difference time-domain (FDTD) approach in two-dimensional (2D) cylindrical coordinates. In their formulation, only the transmitter borehole was included in the model, and the antennae were simulated as point vertical electric dipoles. Ernst et al. (2005) further developed this algorithm to allow for detailed modeling of a realistic, finite-length transmitter antenna. Ellefsen and Wright (2005) employed a similar approach to examine the radiation patterns of realistic borehole GPR antennae. With these methods, much can be learned about the effects of the borehole, subsurface heterogeneity, and antenna characteristics on crosshole GPR radiation.

We present an algorithm to efficiently simulate borehole GPR transmission in heterogeneous media. This is accomplished using FDTD modeling in 2D cylindrical coordinates. The algorithm can be easily implemented perfectly matched layers for absorbing boundaries, frequency-dependent media, and finite-length transmitter antenna.

2. FDTD Modeling in 2D Cylindrical Coordinates

We start with the following Maxwell's equations

$$\frac{\partial \mathbf{D}}{\partial t} = \nabla \times \mathbf{H} \tag{1}$$

$$\mathbf{D}(\omega) = \varepsilon_0 \cdot \varepsilon_r^*(\omega) \cdot \mathbf{E}(\omega) \tag{2}$$

$$\frac{\partial \mathbf{H}}{\partial t} = -\frac{1}{\mu_0} \nabla \times \mathbf{E} \tag{3}$$

where $\mathbf{D}$ is the electric flux density, $\mathbf{E}$ is the electric field, $\mathbf{H}$ is the magnetic field, ε_0 and μ_0 are dielectric permittivity and magnetic permeability in free space, respectively, and

$$\varepsilon_r^*(\omega) = \varepsilon_r + \frac{\sigma}{j\omega\varepsilon_0} \tag{4}$$

where ε_r is the relative dielectric constant, and σ is the conductivity. In this formulation, it is assumed that the materials being simulated are nonmagnetic; that is $\mathbf{H} = \mathbf{B}/\varepsilon_0$, where $\mathbf{B}$ is the magnetic induction. There is a reason for using this formulation: equations (1) and (3) remain the same regardless of the

material; any complicated mathematics stemming from the material is in equation (2). The solution of equation (2) can be viewed as a digital filtering problem (Sullivan, 2000), and the simulation of frequency-dependent media, for example, can be easily addressed.

We further normalize Maxwell's equations by substituting

$$\mathbf{E} = \sqrt{\frac{\varepsilon_0}{\mu_0}}\tilde{\mathbf{E}} = 120\pi\tilde{\mathbf{E}} \tag{5}$$

$$\mathbf{D} = \frac{1}{\sqrt{\varepsilon_0\mu_0}}\tilde{\mathbf{D}} = c_0\tilde{\mathbf{D}} \tag{6}$$

where c_0 is the speed of light. This is a system called Gaussian units. The reason for using it is simplicity in the formulation. The electric and magnetic fields have the same order of magnitude. This has an advantage in formulating the perfectly matched layer (PML), which is a crucial part of FDTD simulation.

The core of our modeling approach is the FDTD solution of Maxwell's equations in 2D cylindrical coordinates presented by Holliger and Bergmann (2002). In this formulation, rotational symmetry about the vertical z-axis is assumed so that Maxwell's equations can be separated into the transverse electric (TE) and transverse magnetic (TM) modes, which are two sets of coupled partial-differential equations involving the (E_ρ, H_ϕ, H_z) and (E_ρ, E_z, H_ϕ) components, respectively. For crosshole GPR modeling where the antennae are oriented parallel to the z-axis, only the TM-mode equations are required. Dropping the ~ notation, Maxwell's equations are reduced in TM mode to

$$\frac{\partial D_\rho}{\partial t} = -c_0\frac{\partial H_\phi}{\partial z} \tag{7}$$

$$\frac{\partial D_z}{\partial t} = c_0\left[\frac{1}{\rho}\frac{\partial(\rho H_\phi)}{\partial \rho}\right] \tag{8}$$

$$D(\omega) = \varepsilon_r^* \cdot E(\omega) \tag{9}$$

$$\frac{\partial H_\phi}{\partial t} = c_0\left(\frac{\partial E_z}{\partial \rho} - \frac{\partial E_\rho}{\partial z}\right) \tag{10}$$

These are solved numerically in the time domain using a leap-frog, staggered-grid approach, which involves offsetting the electric- and magnetic-field components so that the finite-difference approximations of all partial derivatives are centered in both space and time (Yee, 1966). Stepping forward in time is accomplished by alternately updating the electric and magnetic fields. All updates are explicit.

We locate our field components in space identically to Holliger and Bergmann (2002) to avoid singularity problems on the z-axis. We also use second-order-accurate finite-difference approximations for all derivatives, which mean that 10 grid-points per minimum wavelength are needed to control numerical dispersion. We choose the time step according to the Courant numerical stability criterion (Holliger and Bergmann, 2002). Higher-order approximations can be used for the spatial and/or temporal derivatives in our code, with a moderate increase in code complexity, in order to decrease the needed number of field points and thus reduce computing time (e.g., Bergmann et al., 1999).

3. Numerical Results

For numerical simulations we use a finite-difference grid consisting of 110×200 cells and uniform cell width of $\Delta\rho = \Delta z = 1$ cm. The borehole has a diameter of 5 cm, and the antenna has a length of 20 cm. We implement PML absorbing boundaries in cylindrical coordinates to prevent reflections from the top, bottom, and right-hand sides of the simulation grid (Berenger, 1994; Sullivan, 2000).

With the assumed cylindrical symmetry, the transmitter antenna and its borehole, which are centered on the z-axis, can be explicitly and accurately represented with the above approach. We use a dipole antenna as the source. It consists of two metal arms. A dipole antenna functions by having current run through the arms, which results in radiation. FDTD simulates a dipole in the following way: The metal of the arms is specified by setting its conductivity to infinite in the cells corresponding to metal. This insures that the corresponding E_z field at this point remains zero, as it would if that point were inside metal. The source is specified by setting the E_z field in the gap, the cell in between the two arms, to a certain value. For simplicity, we specify a Gaussian pulse as the source.

We base our analyses on a simple model: air-filled borehole in a homogeneous medium ($\varepsilon = 4\varepsilon_0$, $\sigma = 0.001$ S/m). Figure 1 shows results of a simulation for the homogeneous model. As the wave reaches PML, which is eight cells on top, bottom, and right-hand sides, it is absorbed. The effectiveness of PML is apparent in the right figure because the image would not be concentric circles if the outgoing wave were partially reflected.

Figure 2 shows radargrams collected along a vertical line at a distance of 1 m from the symmetric axis for the homogeneous reference model. No reflection from the artificial boundaries is not recognized. Figure 3 shows the result of a simulation with a model with a small air-filled cavity. Note that a portion of the wave propagates into the cavity and a portion is reflected, in keeping with basic EM theory.

4. Concluding Remarks

We have presented a finite-difference solution of Maxwell's equations in cylindrical coordinates that is suitable for modeling borehole GPR data. This algorithm was used to model the EM wavefield radiated from a vertical electric antenna located in a borehole filled with air. Major simplifications made in this study were that only the radiation pattern of the transmitter was accounted for explicitly and that the receiving antenna was approximated by an infinitesimal electric dipole. The radiation pattern of a vertical antenna located in a water-filled borehole is severely distorted with respect to the corresponding reference pattern in a homogeneous full-space due to waveguide effects. Given that most shallow boreholes are at least partially water-filled, this has potentially serious implications for the interpretation of borehole GPR data. Further complications of the radiation pattern, regardless of the medium filling the borehole, must be expected to arise from vertical stratification and/or lateral heterogeneity of electric parameters in the shallow subsurface.

Acknowledgment: This work was supported by Pukyong National University Research Foundation Grant in 2005 (PR-2005-018).

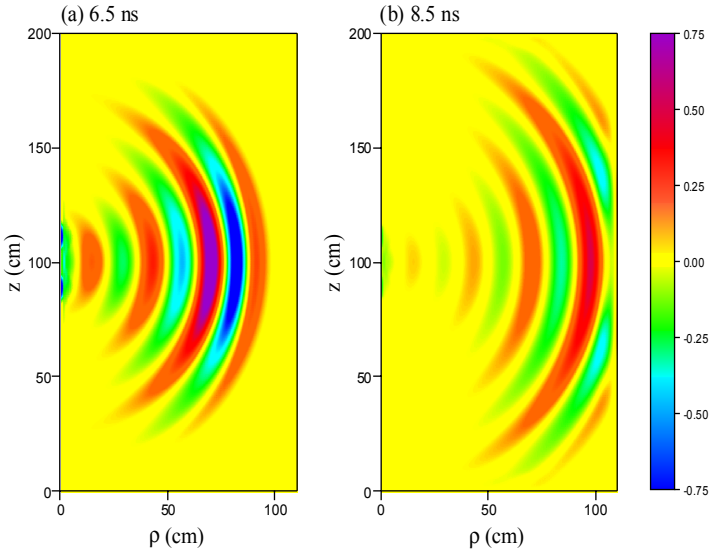

Fig. 1. Snapshots of E_z fields at 6.5 ns (a) and 8.5 ns (b) for a homogeneous model. Outgoing waves, initiated from a Gaussian pulse at z = 100 cm in the air-filled borehole, remain concentric (a). Only when the wave gets within eight points of the top, bottom, and right-hand edges, which are inside PML, does distortion start to occur (b).

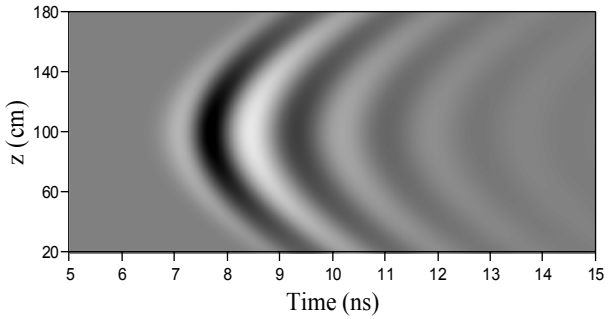

Fig. 2. Radargrams consisting of the E_z-component of the EM wavefield radiated from a 20 cm vertical antenna for a homogeneous model and an air-filled borehole. The data are collected along a vertical line at a distance of 1 m from the symmetry axis.

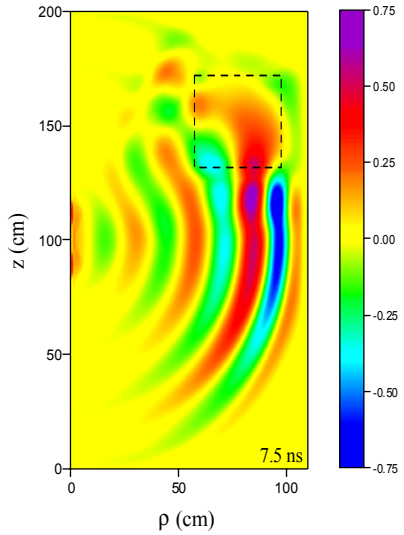

Fig. 3. Snapshots of E_z fields at 7.5 ns. The outgoing wave moves faster inside the air-filled cavity, denoted by dotted rectangle. Reflections are generated at the cavity boundary.

References

Alumbaugh, D., and P. Y. Chang, 2002, Estimating moisture contents in the vadose zone using cross-borehole ground-penetrating radar: A study of accuracy and repeatability: Water Resources Research, **38**, 1309, doi:10.1029/2001WR000754.

Berenger, J. P., 1994, A perfectly matched layer for the absorption of electromagnetic waves: Journal of Computational Physics, **114**, 185–200.

Bergmann, T., J. O. Blanch, J. O. A. Robertsson, and K. Holliger, 1999, A simplified Lax-Wendroff correction for staggered-grid FDTD modeling of electromagnetic wave propagation in frequency-dependent media: Geophysics, **64**, 1369–1377.

Day-Lewis, F. D., J. W. Lane, J. M. Harris, and S. M. Gorelick, 2003, Time-lapse imaging of saline tracer transport in fractured rock using difference radar attenuation tomography: Water Resources Research, **39**, 1290, doi:10.1029/2002WR001722.

Ellefsen, K. J., and D. L. Wright, 2005, Radiation pattern of a borehole radar antenna: Geophysics, **70**, K1–K11.

Ernst, J. R., K. Holliger, and H. Maurer, 2005, Realistic FDTD modelling of borehole georadar antenna radiation: Methodology and application: Near Surface Geophysics, SEG.

Fullagar, P. K., D. W. Livelybrooks, P. Zhang, and A. J. Calvert, 2000, Radio tomography and borehole radar delineation of the McConnell nickel sulphide deposit, Sudbury, Ontario, Canada: Geophysics, **65**, 1920–1930.

Holliger, K., and T. Bergmann, 2002, Numerical modeling of borehole georadar data: Geophysics, **67**, 1249–1257.

King, R. W. P., and G. S. Smith, 1981, Antennas in matter: Fundamentals, theory, and applications: MIT Press.

Moran, M. L., and R. J. Greenfield, 1993, Radar signature of a 2.5-D tunnel: Geophysics, **58**, 1573–1587.

Moysey, S., and R. J. Knight, 2004, Modeling the field-scale relationship between dielectric constant and water content in heterogeneous systems: Water Resources Research, **40**, W03510, doi:10.1029/2003WR002589.

Olhoeft, G. R., 1988, Interpretation of hole-to-hole radar measurements: 3rd Symposium on Tunnel Detection, Proceedings, 616–629.

Olsson, O., L. Falk, O. Forslund, L. Lundmark, and E. Sandberg, 1992, Borehole radar applied to the characterization of hydraulically conductive fracture zones in crystalline rock: Geophysical Prospecting, **40**, 104–116.

Pratt, R. G., and M. H. Worthington, 1988, The application of diffraction tomography to cross-hole seismic data: Geophysics, **53**, 1284–1294.

Sato, M., and R. Thierbach, 1991, Analysis of a borehole radar in cross-hole mode: IEEE Transactions on Geoscience and Remote Sensing, **29**, 899–904.

Sullivan, D. M., 2000, Electromagnetic Simulation Using The FDTD Method: IEEE Press.

Tronicke, J., K. Holliger, W. Barrash, and M. D. Knoll, 2004, Multivariate analysis of cross-hole georadar velocity and attenuation tomograms for aquifer zonation: Water Resources Research, **40**, W01519, doi:10.1029/2003WR002031.

Williamson, P. R., and M. H. Worthington, 1993, Resolution limits in ray tomography due to wave behaviour: Geophysics, **58**, 727–735.

Yee, K. S., 1966, Numerical solution of initial boundary value problems involving Maxwell's equations in isotropic media: IEEE Transactions on Antennas and Propagation, **14**, 302–307.

Zhou, C., W. Cai, Y. Luo, G. Schuster, and S. Hassanzadeh, 1995, Acoustic wave-equation traveltime and waveform inversion of crosshole seismic data: Geophysics, **60**, 765–773.